NJC

ROYAL SOCIETY OF CHEMISTRY

PAPER

View Article Online
View Journal | View Issue

Cite this: *New J. Chem.*, 2023, **47**, 4409

Eco-friendly synthesis of ZnO-nanoparticles using *Phoenix dactylifera* L., polyphenols: physicochemical, microstructural, and functional assessment

Johar Amin Ahmed Abdullah, *[a] Mercedes Jiménez Rosado, [a] Antonio Guerrero [a] and Alberto Romero [b]

Recently, nanoparticle (NP) synthesis has evolved into a green nanotechnology field, requiring more methods for the eco-synthesis of nanoparticles due to the high costs of other chemical–physical methods. Among the most commonly used nanomaterials, ZnO-NPs are highly valuable due to their specific, thermal, optical, and electronic features. Thus, the main objective of this work was to investigate the green synthesis of ZnO-NPs employing the *Phoenix dactylifera* L., extract, which is rich in polyphenols, as a reducing agent. In this way, the effect of the concentration of both the precursors and the reducing agent was evaluated. The NPs were characterized and compared through X-ray diffraction (XRD), transmission electron microscopy (TEM), scanning electron microscopy (SEM) and Fourier infrared transformation spectroscopy (FTIR). Additionally, we evaluated the antioxidant properties (TAC and DPPH) and antibacterial activity of these nanoparticles against Gram-positive *Staphylococcus aureus* (*S. aureus*) and Gram-negative Escherichia coli (*E. coli*) pathogenic strains. The results show that it is possible to obtain ZnO-NPs using a green reducing agent (polyphenol extract), presenting a particle size between 18.1 and 61.6 nm. In addition, this synthesis highlighted the antioxidant and antibacterial activities of these nanoparticles. In conclusion, this method could be a suitable substitute for typical toxic methods for the synthesis of metallic nanoparticles.

Received 9th January 2023,
Accepted 25th January 2023

DOI: 10.1039/d3nj00131h

rsc.li/njc

Introduction

Interest in nanomaterials has increased due to their special characteristics that allow them to be applied in a wide range of fields and applications, including the chemical, medical, pharmaceutical, mechanical, and technological industries.[1] Almost all academic disciplines consider this to be one of the most prominent areas of research and development,[2] as they have many unique characteristics, including strength, lightweight, excellent chemical reactivity, and a very small size with a high surface area and stability. Among the most commonly used nanomaterials, zinc oxide nanoparticles (ZnO-NPs) have gained considerable interest in scientific and medical communities.[3] It is a very valuable material with multiple properties suitable for high technology applications, such as light-emitting diodes, optical detectors, chemical and biological sensors, energy aggregators (e.g., solar cells), nano-molders and electromagnetics. This is due to their highly attractive chemical properties such as a high electrochemical correlation coefficient and high photochemical stability, as well as their excellent electronic, electrical, and physical properties.[4] ZnO-NPs have not only been used in these fields; they also play an important role in other fields, such as cosmetics and drug delivery, where they are widely used to treat various skin diseases due to their potential UV-ray absorption (e.g., as UV radiation deterrents in sunscreens), antimicrobials and many medical products.[5,6] On the other hand, nanoparticles can be tailored to be used against specific diseases, being of special interest in medicine, where they can provide new ways of treating diseases that are hard to target due to size constraints.[7] In addition, ZnO-NPs are considered safe and non-toxic according to the U.S. Food and Drug Administration, and they can be used in different medical-industrial sectors.[8] Furthermore, they are toxic to cancer cells, bacteria and leukemia cells, being attractive as drug delivery agents and gene delivery biosensors, as well as in cancer treatments.[9] It is safe to say that there have been no known human diseases caused by geometric nanoparticles.[10]

Zinc oxide nanoparticles are scaled with a diameter smaller than 100 nm. The different manufacturing methods result in

[a] *Departamento de Ingeniería Química, Escuela Politécnica Superior, Universidad de Sevilla, 41012, Sevilla, Spain. E-mail: jabdullah.us.es; Tel: +34954557179*
[b] *Departamento de Ingeniería Química, Facultad de Física, Universidad de Sevilla, 41012, Sevilla, Spain*

different physical and chemical properties of ZnO-NPs.[11] There are several methods to produce zinc oxide nanoparticles: sedimentation processes, hydrothermal methods, laser excision molecules, sol–gel methods, electrochemical deposits, chemical steam deposition, ultrasound, thermal decomposition, microwave-assisted combustion methods, combustion methods, two-step thermal-mechanical synthesis, precipitation, aluminium oxide coating, and electrical deposition using different solution concentrations, pH values, and washing media.[12] Nevertheless, these methods are costly and regrettably dependent on the use of toxic chemicals.[13–15] Thus, recently, many studies have focused on green ways to produce nanoparticles from noble metals that are simple, cost-effective, and repeatable.[16] The relevance of these green technologies is that they are cost-effective, non-toxic, rapid, and lead to the formation of highly crystalline nanoparticles in a variety of sizes and shapes.[17] To develop ecologically safe technologies, mostly plant or fruit extracts are utilized.[18] They contain high concentrations of polyphenols, which reduce the metal salts into high-purity nanoparticles through their unique features (reducing properties, hydrogen bonding ability, nucleophilic nature, polarizability, acidity, chelating properties, *etc*).[19] These properties have led to the production of nanoparticles, thanks to their mentioned properties and suitable biocompatibility, and they have been thus vastly employed in biomedical applications.[20–22]

Date palm (*Phoenix dactylifera* L.) is an ancient tropical and subtropical fruit plant that belongs to the Aceraceae family and is grown in the Arabian Peninsula (Yemen, Oman, Qatar, Saudi Arabia, the United Arab Emirates (UAE), and Kuwait, as well as the southern regions of Jordan and Iraq) and Northern Africa (Egypt, Sudan, Libya, Tunisia and Algeria).[23–25] *Phoenix dactylifera* L. provides food, medicine, construction materials and fuel, and hence it is called the tree of life. It is an extremely widespread tree with a wide range of nutritional, economic, and medicinal applications, including food additives, antimicrobials, antilipidemic and anti-diabetes drugs[19,24] *Phoenix dactylifera* L. has previously been investigated for its high levels of phytochemicals (e.g., polyphenols, flavonoids, aldehydes, terpenoids, fatty acids alkaloids, *etc*).[26–28] A number of metal oxide nanoparticles have been synthesized using this plant species, such as iron oxide, gold, silver, nickel nanoparticles, *etc*.[24,29]

This study aims to investigate the green synthesis of ZnO-NPs employing *Phoenix dactylifera* L. extract rich in polyphenols as a reducing agent. In this way, the effect of both precursor and reducing agent concentrations was evaluated. Further investigation involved X-ray diffraction (XRD), transmission electron microscopy (TEM), scanning electron microscopy (SEM) and Fourier infrared transformation spectroscopy (FTIR) studies. Furthermore, the antioxidant (TAC and DPPH) and antibacterial (*S. aureus* and *E. coli*) activities of these nanoparticles were compared.

Materials and methodology

Materials

Zinc chloride ($ZnCl_2$), methanol (CH_3OH), ethanol (CH_3CH_2OH), sulfuric acid (H_2SO_4), sodium phosphate (Na_2HPO_4), ammonium molybdate ($(NH_4)_3PMo_{12}O_{40}$), gallic acid ($C_7H_6O_5$), hydrochloric acid (HCl), 2,2-diphenyl-1-picrylhydrazyl (DPPH), dimethyl sulfoxide anhydrous (DMSO) 99.9% (C_2H_6SO) were purchased from Sigma Aldrich (Darmstadt, Germany). Throughout the study, only analytical-grade chemicals and reagents were used.

Phoenix Dactylifera L. leaves were harvested from Seville (Spain), at an average temperature of 19 ± 4 °C (with maximum and minimum temperatures of 36 °C and 6 °C, respectively), at an average RH (relative humidity) of 53% (according to the NOAA; National Oceanic and Atmospheric Administration). Then, they were left to dry in the shade for 44 days at a mean temperature of 22 ± 3 °C and an average RH of 35%. This protocol was developed from a previous study, in which the *Phoenix dactylifera* L. leaves were dried at different temperatures (25–150 °C) until a constant water loss percentage was achieved. The most favorable results were obtained at room temperature, where a higher content of polyphenols and the formation of smaller nanoparticles with higher crystallinity were observed.[30]

Phoenix dactylifera L. extraction was performed according to previous studies with modifications.[29,30] Briefly, 30 g of powdered *Phoenix dactylifera* L. was extracted using distilled water (300 mL) through Soxhlet extraction at 98 °C for 8 h. The extraction yield was 53.8 ± 0.8% corresponding to 38.6 ± 1.7 (mg GAE/g extract) of the total polyphenol content (TPC). The extraction yield and TPC calculation are more detailed in a previous study.[30]

Nanoparticle synthesis

ZnO-NP synthesis was performed according to previous studies with modifications.[29,30] Briefly, 20 mL of the extract was transferred dropwise into 20 mL of zinc chloride ($ZnCl_2$) solution. Three different concentration ratios ([2 : 1], [1 : 1] and [1 : 2]) for the concentrations 0.1, 0.2, 0.4, 0.5, 1 and 2 M were paired and evaluated. The resulting solutions were then transferred into beakers, heated at 50 °C under stirring for 2 h, and then purified by filtering through Whatman no 1 papers and washed with distilled water at least three times to remove dirt and particles suspended in the mix. The samples were pretreated in an oven at 100 °C for 8 hours, followed by a final heat treatment at 500 °C for 5 h to remove any residual material from the sample.

It is worthwhile to highlight that nanoparticle treatment involves two critical heating steps: the first step involves the use of a drying oven at a regulated temperature (60–190 °C) in which airflow is used to transfer heat (ensuring intense heat transmission and thereby faster drying) for heating, drying (extraction of large amounts of water from samples), hardening and sterilizing materials and chemical salts. During the next step, a muffle is used to reach very high temperatures, where heat is transferred by radiation, providing continuous heat for the processing of materials as well as the destruction of organic substances (combusting organic substances and removing impurities).

ZnO-NP characterization

X-ray diffraction (XRD). XRD patterns were obtained using a Brand diffractor (Bruker Model D8 advance A25 with Cu anode) to confirm the presence of crystalline phases in the sample. The crystalline size of ZnO-NPs and the crystallinity degree were calculated by applying the Debye-Scherrer formula, following the description given in previous studies.[29,31] The diffractograms were obtained in the range of 2θ (°) = 15–70.

Transmission electron microscopy (TEM). A TEM study was performed to determine the crystalline characteristics of the nanoparticles, as well as their size. It was carried out using a Talos S200 microscope (FEI, USA) at 200 kV. Elemental information of the ZnO-NPs was labelled using Image-J free software.[32]

Scanning electron microscopy (SEM). SEM was primarily used to gather the size (average diameter distribution) and the structural morphology of the ZnO-NPs. This was carried out at an acceleration voltage of 10 kV using a Zeiss EVO scanning electron microscope (USA). To compare the samples, they were scanned under various magnifications. Image-J free software was used to label elemental information of the ZnO-NPs.[32]

Fourier transform infrared spectroscopy (FTIR). The vibration modes of the bonds present in the ZnO-NPs from 4000 to 400 cm^{-1} were used to gather information on the nanoparticle (NP) structure using an FTIR spectrometer (Hyperion 100 Spectrometer, Bruker, USA). The spectrometer was configured in the transmittance mode using a DTGS-KBr sensor. It is possible to identify three distinct zones at the global level: absorbance bands associated with alkyl chains on the surface (3000–2800 cm^{-1}), the COO– group in oleates (1800–900 cm^{-1}), and the Zn–O bonds in Zn–O (800–400 cm^{-1}).[33]

Antioxidant activity (TAC and DPPH). The antioxidant activity was determined either through the products of oxidation or from the capacity of the reaction models to trap radicals. Two different tests have been used: the total antioxidant activity of phosphomolybdate (TAC) and the free radical scavenging of the DPPH test.

The TAC is used to analyze oxidation compounds, thereby searching for functional groups in derivatives of the original constituents (carbonyl compounds of aldehydes, ketones, dicarbonyls, *etc.*). The DPPH test determines how many radicals are trapped in relation to the amount of antioxidants applied.

The TAC and DPPH tests were carried out using the protocol described in a previous study without modifications.[29] Briefly, for TAC analysis, 2 mL of Zn-NPs (dispersed in HCl) was mixed with 2 mL of reagent (0.6 M H_2SO_4, 28 mM Na_2HPO_4 and 4 mM $(NH_4)_3PMo_{12}O_{40}$). Then, the mixture was incubated in a water bath at 95 °C for 90 min. The absorbance was read at 695 nm using spectrophotometry, and gallic acid was used as a reference. The DPPH test was conducted by mixing 2 mL of ZnO-NPs/DMSO solution dispersed in different concentrations (0.125, 0.25, 0.5, 1, 2, and 4 mg mL^{-1}) with 2 mL of DPPH methanolic solution. After incubating the mixtures for 0.5 hours, the absorbance at 517 nm was determined. A mixture of DPPH and DMSO was used as a control. The inhibition percentage IP (%) of the tested samples was calculated according to eqn (1)

$$\mathrm{IP}(\%) = \left(\frac{A_D - A_{Da}}{A_D}\right) \times 100 \quad (1)$$

where A_D is the absorbance value of the oxidized solution (without the ZnO-NP antioxidant agent) and A_{Da} is the absorbance after adding the ZnO-NP antioxidant agent. Moreover, the IC_{50} (the necessary antiradical concentration to inhibit 50% of DPPH) was determined using GraphPad Prism 9 software (Windows GraphPad Prism, 9.0.0, San Diego, California, USA, https://www.graphpad.com).[29]

Antibacterial activity. The antimicrobial activity of the as-selected ZnO-NPs (optimized through TAC and DPPH values) was evaluated using an agar diffusion experiment as described by Behera *et al*. with slight modification.[34] In this way, holes of diameter 9 mm were made in agar gels inoculated with *Staphylococcus aureus* (*S. aureus*) and *Escherichia coli* (*E. coli*) using the end of a cone-shaped micropipette tip as a perforator. After that, the holes were filled with 20 μL (50 mg mL^{-1}) of ZnO-NPs dispersed in distilled water (using ultrasound for 20 min) and 10 μL of gentamicin (50 μg mL^{-1}) in wells of diameter 2 mm was used as a standard.

The antibacterial activity was assessed by measuring the inhibition diameters surrounding the ZnO-NPs solution after 24 and 48 h of incubation at 37 °C using Image-J software.[35]

Statistical analysis. GraphPad Prism9 and IBM SPSS Statistics 26 software were used for statistical analysis. One-way ANOVA was applied to estimate the significance of the differences between observations. At least three replicates of the data were used to calculate the mean ± SD. The significance level was estimated using HSD Tukey statistical analysis ($p < 0.05$).

Results and discussion

XRD

The X-ray diffractograms of the ZnO-NPs synthesized from *Phoenix dactylifera* L. extract using different concentrations are depicted in Fig. 1.

The peaks observed at 2θ (°) = 31.7, 34.4, 36.3, 47.5, 56.6, 62.9, 66.4, 67.9 and 69.1 could be attributed to the crystallographic reflection's planes (100), (002), (101), (102), (110), (103), (200), (112), and (201), derived from the hexagonal structure of zinc oxide; space group: *P*63*mc* (186) with standard crystallographic parameters a = 3.2501 Å b = 3.2501 Å, and c = 5.2071 Å (JCPDS no. 01-079-2205 standard zincite ZnO powder diffraction pattern).[36]

The well-defined and sharper peaks in the XRD of ZnO-NPs reveal that the ZnO-NPs exhibit various levels of crystallinity. The crystal sizes and crystallinity degrees calculated using the Debye-Scherrer equation are reported in Table 1.

For the [1 : 2] and [2 : 1] ratios, nanoparticle size decreased at lower concentrations of both the precursor and the reducing agent (Table 1), possibly due to lower agglomeration or aggregation. Similar results reported by Kodama *et al*. showed aggregation when [OH] was high.[37] Green synthetic ZnO-NPs

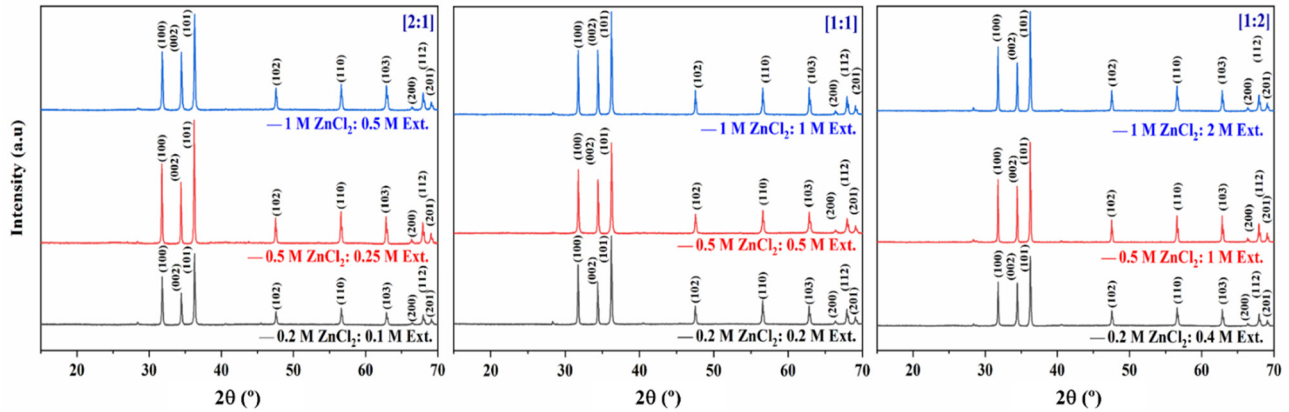

Fig. 1 XRD spectrum of the ZnO-NPs (JCPDS standard) synthesized using an eco-friendly *Phoenix dactylifera. L, extract* in different ratios ([2 : 1], [1 : 1] and [1 : 2]) and concentrations (0.1, 0.2, 0.4, 0.5, 1 and 2 M).

Table 1 Results obtained for different parameters of the ZnO-NPs synthesized using an eco-friendly *Phoenix dactylifera* L, extract in different ratios ([2 : 1], [1 : 1] and [1 : 2]) and concentrations (0.1, 0.2, 0.4, 0.5, 1 and 2 M): mean diameter (from XRD measurements, TEM, and SEM images), mean length (from SEM), crystallinity percentage, and antioxidant activity (TAC and IC_{50} DPPH free radical)

Ratio	$ZnCl_2$: Ext [M]	D_{XRD} (nm)	D_{TEM} (nm)	D_{SEM} (nm)	Length (nm)	Crystallinity %	TAC (mgGAE mg^{-1} NPs)	IC_{50} (mg ml^{-1})
2 : 1	0.2 : 0.1	19.7 ± 1.2^{i}	18.6 ± 0.5^{h}	18.1 ± 0.5^{i}	108 ± 33^{cd}	83.5^{h}	4.1 ± 0.0^{ab}	2.04 ± 0.1^{e}
	0.5 : 0.25	31.4 ± 1.4^{f}	30.1 ± 0.3^{e}	31.5 ± 0.3^{f}	216 ± 107^{ab}	86.3^{f}	1.1 ± 0.1^{c}	4.24 ± 0.1^{d}
	1 : 0.5	38.4 ± 1.0^{d}	39.0 ± 0.1^{c}	38.3 ± 0.6^{d}	197 ± 56^{bc}	89.0^{d}	0.5 ± 0.0^{c}	5.20 ± 0.3^{b}
1 : 1	0.2 : 0.2	26.7 ± 0.1^{h}	19.8 ± 0.2^{g}	25.1 ± 0.8^{h}	151 ± 22^{bc}	83.6^{i}	2.3 ± 1.6^{bc}	1.38 ± 0.0^{f}
	0.5 : 0.5	36.4 ± 0.6^{e}	37.3 ± 0.4^{d}	36.8 ± 0.9^{e}	291 ± 37^{a}	87.0^{e}	1.6 ± 0.1^{c}	4.83 ± 0.3^{c}
	1 : 1	44.3 ± 0.5^{b}	41.6 ± 0.9^{b}	46 ± 0.7^{b}	219 ± 31^{ab}	92.8^{b}	1.4 ± 1.9^{c}	6.77 ± 0.3^{a}
1 : 2	0.2 : 0.4	28.3 ± 0.9^{g}	28.5 ± 0.8^{f}	28.7 ± 0.6^{g}	48 ± 15^{d}	84.2^{g}	1.3 ± 0.1^{c}	1.17 ± 0.1^{f}
	0.5 : 1	41.2 ± 1.2^{c}	40.0 ± 0.1^{c}	40.4 ± 1.4^{c}	109 ± 36^{cd}	92.2^{c}	$2.7 \pm 2.4b^{c}$	2.07 ± 0.1^{e}
	1 : 2	49.8 ± 1.7^{a}	61.6 ± 1.3^{a}	49.6 ± 0.3^{a}	120 ± 42^{cd}	93.2^{a}	5.4 ± 0.4^{a}	2.17 ± 0.1^{e}

Note: Different superscript letters (a–i) within a column indicate significant differences among mean observations ($p < 0.05$).

tended to be larger in size at higher concentrations of both the precursor and extract reducing agent, which may be attributed to the competition between functional groups of the extract and zinc ions, and thus the reduction rate would also increase.[17] This could indicate that the 0.1 M concentration of the extract is just right for obtaining the lowest crystallite sizes. Similar results have been found in the literature.[38–40] For the [1 : 1] ratio, the size and number of nanoparticles increased with the precursor concentration. Similar results were obtained in other studies; for example, Fuad *et al.* found that an increase in the concentration of the precursor from 30 to 35 mM led to an increase in nanoparticle size from 44.6 to 58.9 nm.[41] Jon *et al.*, who synthesized gold nanoparticles from *Zea Mays extract* using chloroauric acid ($HAuC_{l4}$) as a precursor, found that the size of the nanoparticles increased from 6 to 50 nm with an increase in the precursor concertation from 0.5 to 5 mM.[42] Furthermore, the sizes of the synthesized ZnO-NPs using *Phoenix dactylifera* L. in this study were much smaller than those obtained using other methods reported in the literature; for example, Mohammad *et al.*, using the sol–gel process at three different ratios of 3 : 1, 1 : 1 and 1 : 3, obtained ZnO nanoparticle sizes of 160, 220 and 250 nm, respectively.[43] The synthesis mechanism for the ZnO nanoparticles is shown in Fig. 2.

Phoenix dactylifera. L, extract, as a good source of polyphenols (phytochemicals), reduces metal precursors ($ZnCl_2$) to metal nanoparticles (ZnO-NPs). Polyphenols are non-toxic antioxidants that can reduce precursors and stabilize the obtained nanoparticles without generating toxic wastes.[19,44] Phenolic compounds, as essential phytochemicals, contribute to reduction processes. Thus, the concentration of these reducing agents (phenolic compounds) varies for different types of plant extracts. As a result, leaf extract concentration affects nanoparticle synthesis.[45] Studies propose that the metal ions after reduction with phytochemicals may be covered in an organic

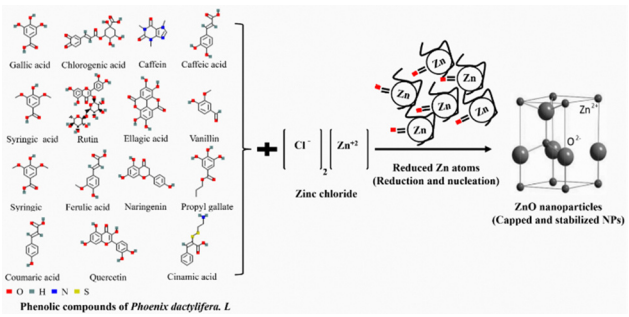

Fig. 2 Mechanism for the eco-friendly synthesis of ZnO nanoparticles.

compound in three phases for stabilization: (i) Activation phase: involves precursor formation, metal ion reduction (e.g., neutralization reactions) and metal ion nucleation; (ii) growth phase: contributes to nanoparticle stability; and (iii) termination phase: determines the shape of nanoparticles, where ageing processes such as coarsening and aggregation take place.[28,46,47]

Nucleation kinetics is correlated with chemical reaction kinetics and molecular mechanisms in this case. As a result of the colloidal green synthesis of ZnO from $ZnCl_2$ and R–OH (extract phenolic compounds) in water, the following chemical reaction can be described:[47]

$$n\mathrm{ZnCl_2} + 2n\mathrm{R{-}OH} + l\mathrm{H_2O} \rightarrow \mathrm{Zn^{2+}}_n(\mathrm{OH^-})_m(\mathrm{H_2O})_l\mathrm{Cl^-}_k + (2n-k)\,\mathrm{Cl^-} + (2n-m)\,\mathrm{OH^-} + 2n\mathrm{R^+} \rightarrow n\mathrm{ZnO} + (l+n)\,\mathrm{H_2O} + 2n\mathrm{R{-}Cl} \quad (2)$$

As can be seen, the zinc–ligand molecule acts as a nucleation precursor, with $2n = m + k$ when a zero-charge precursor is present. Precursor formation kinetics, which show a rapid behavior, increase the supersaturation with time and initiate a burst of nucleation if a certain threshold is reached. The supersaturation decreases in response to the relative velocities of precursor nucleation and the amount of the total material present in the system, which, in turn, delays and eventually stops the nucleation. When the precursor formation rate is slow, nucleation can take place at constant supersaturation for an extended time.[47]

Plant polyphenols enable metals to form their metal oxides and make them reach the growth and stabilization phases. Finally, by binding metal ions to oxygen, nanoparticles with a defined shape are formed in the final treatment at annealing temperatures.[28,46]

Table 1 also shows the relationship between the crystallinity and the variation in the concentration ratio [precursor: extract reducing agent], which explains that the higher the percentage of the extract (reducing agent), the greater the crystallinity. This is due to the fact that ZnO-NPs at high concentrations (both the precursor and extract reducing agent) generally form crystals containing more ZnO than at low concentrations.[48]

TEM

Fig. 3 shows TEM images of the synthesized ZnO-NPs with different morphologies and the histograms of nanoparticle size distributions, where they were fitted by applying a normal curve.

Accordingly, nanoparticle average diameters ranged between 18.6 ± 0.5, which corresponds to the system with the lowest content of the precursor and reducing agent, and 61.6 ± 1.3 nm, obtained for the highest concentration of both agents (Table 1).

As can be observed, the [2 : 1] ratio revealed numerous nanoparticle aggregates and cubic particles, which may indicate the competition between functional groups of the extract and zinc ions on the ZnO-NP surface, thus leading to an increase in the reduction rate.[17] At a [1 : 1] ratio, weakly aggregated, quasi-spherical, cubic, and hexagonal nanoparticles were observed. When the ratio was inversed to [1 : 2] by doubling the extract concentration, the nanoparticles were better dispersed with different shapes, cubic, hexagonal, and spherical structures. This indicates that an increase in reducing agent concentration (*i.e.*, an increase in $-OH^-$) may lead to the production of a large number of zinc hydroxide ions $Zn(OH)_4^{2-}$, leading to ZnO-NP formation, which in turn reduces the growth rate and the interaction between nanoparticles.[49] These results are similar to those of previous studies.[38,50,51] It would be worth trying to confirm these results with another microscopy technique such as SEM.

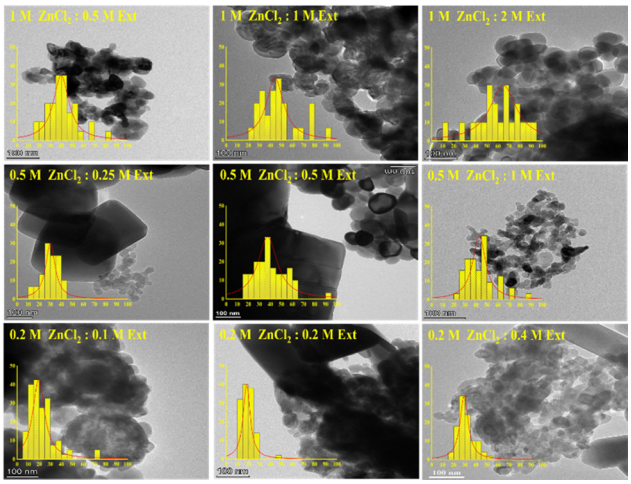

Fig. 3 Transmission electron microscopy (TEM) images of ZnO-NPs synthesized using an eco-friendly *Phoenix dactylifera*. L., extract at different ratios ([2 : 1], [1 : 1] and [1 : 2]) and concentrations (0.1, 0.2, 0.4, 0.5, 1 and 2 M).

SEM

Fig. 4 shows ZnO-NP morphology and nanoparticle size distributions.

Nanoparticles/nanorods presented an average diameter between 18.1 ± 0.5 and 49.6 ± 0.3 nm, from the lowest to the highest reactant contents. Their lengths ranged between 48 nm (for the 0.2 : 0.4 system) and 291 nm (for the 0.5 : 0.5 system) and showed a less regular dependence on the precursor or reducing agent concentrations. Detailed results are shown in Table 1.

At a [2 : 1] ratio, numerous closely packed and larger rod-shaped nanoparticles, with spherical, face-centered rhombohedral, cubic, and hexagonal structures were observed. When the ratio was adjusted to [1 : 1], numerous well-dispersed hexagonal nanorods at lower concentrations, and a few spherical nanoparticles at higher concentrations with slight aggregation/agglomeration were observed. When the ratio was changed to [1 : 2] by doubling the extract concentration, excellently dispersed hexagonal nanorods, as well as cubic and spherical nanoparticles were obtained. Similar results have been reported in previous studies.[17,37,41,48,52] These polygonal or anisotropic structures indicate that the precursor and reducing agent concentrations affect nanoparticle sizes and morphologies. The interactions of nanoparticles with each other resulted

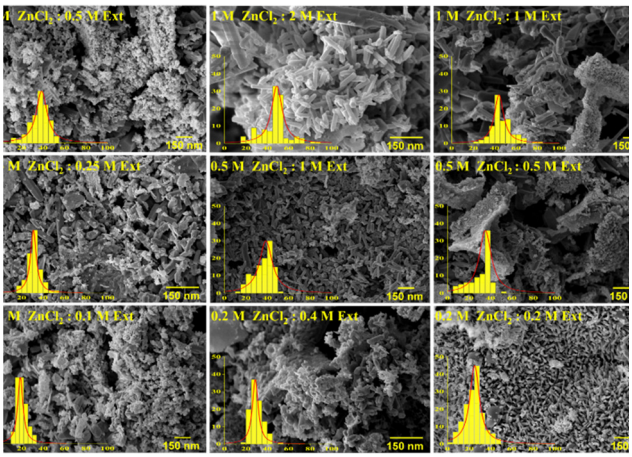

Fig. 4 Scanning electron microscopy (SEM) images of ZnO-NPs synthesized using an eco-friendly *Phoenix dactylifera*. L., extract at different ratios ([2 : 1], [1 : 1] and [1 : 2]) and concentrations (0.1, 0.2, 0.4, 0.5, 1 and 2 M).

in slight agglomeration of NPs in some cases,[52,53] while in other cases they grew and agglomeration occurred due to the phytochemicals present in *Phoenix* extracts acting as stabilizing agents and the ageing effect caused by reflux conditions.[53] As a result of hydrogen bonding (H-bonding) in bioactive molecules, these nanoparticles appeared as aggregates.[32,54,55] It can be noticed that, in general, the nanoparticle sizes obtained from SEM are rather coincident with those obtained from the other two techniques applied (particularly from XRD).

FTIR

FTIR characterization of ZnO-NPs synthesized at different concentrations and concentration ratios is shown in Fig. 5.

The first observation was focused in the range of 800–400 cm^{-1}, which characterizes Zn–O bonds. Peaks observed in the range of 650–400 cm^{-1} are caused by the Zn–O vibrations of ZnO-NPs.[17,51] As can be seen in the whole systems [2 : 1], [1 : 1] and [1 : 2], the low concentrations have led to an increase in absorbance, which may justify the smaller nanoparticles. Similar trends have shown that an increase in absorbance and the band area correlates with smaller particle sizes.[56]

The biomolecules responsible for reducing the metal precursors to ZnO nanoparticles appear in the range of 3500–3200 cm^{-1}, and a band at 3416 cm^{-1} is attributed to the vibrational stretching of OH polyphenolic compounds of *Phoenix dactylifera* L. The bands around 1631.37, 1623.52, and 1635.29 cm^{-1} are attributed to the stretching vibration of C=C and bonds in alkene groups or to aromatic ring deformation, and those which appear around 1733, 1737, and 1741.1 cm^{-1} are assigned to – C=O bonds of aldehydes, ketones and esters, and the bands at 1376.47 1384.31, 1380,39 are associated with ester groups.[57,58] The bands in the range of 1200–1247 cm^{-1} could represent an asymmetric stretching vibration of C–O, typical of polyphenolic compounds.[58] The bonds appearing in the range of 1039–1070 cm^{-1} represent C–O–C stretching vibration of phenolic compounds and polysaccharides.[58] The bonds in the range of 1105–1160 cm^{-1} are assigned to C–O–H in phenolic compounds.[58] The reduction of $ZnCl_2$ with the phenolic compound of *Phoenix dactylifera* L. into ZnO-NPs gave rise to an absorption band around 1643 cm^{-1}, segmented into three peaks at 1653, 1633 and 1623 cm^{-1}.[29] Furthermore, the appearance of bio-components such as phytochemicals (polyphenols, and their derivatives, such as phenolic compounds, flavonoids, tannic acid, phytosterols, *etc.*) in FTIR spectra originated from the extract, which serves as reducing agents of metal ions to nanoparticles due to their oxidation–reduction potential as well as stabilizing and capping agents on nanoparticle surfaces.[59,60]

Antioxidant activity

Table 1 also summarizes the total antioxidant activity (TAC) and IC_{50} for the inhibition of 50% of free radical DPPH. A lower IC_{50} value presents a higher antioxidant activity.

The ZnO-NPs synthesized at [2 : 1] and [1 : 1] ratios were observed to exhibit higher total antioxidant activity at lower concentrations (Table 1), which could be due to the small size of ZnO-NPs and the presence of capping agents,[61] while the highest TAC of ZnO-NPs was generally observed with the ZnO-NPs at the [1 : 2] ratio (Table 1). This could be explained

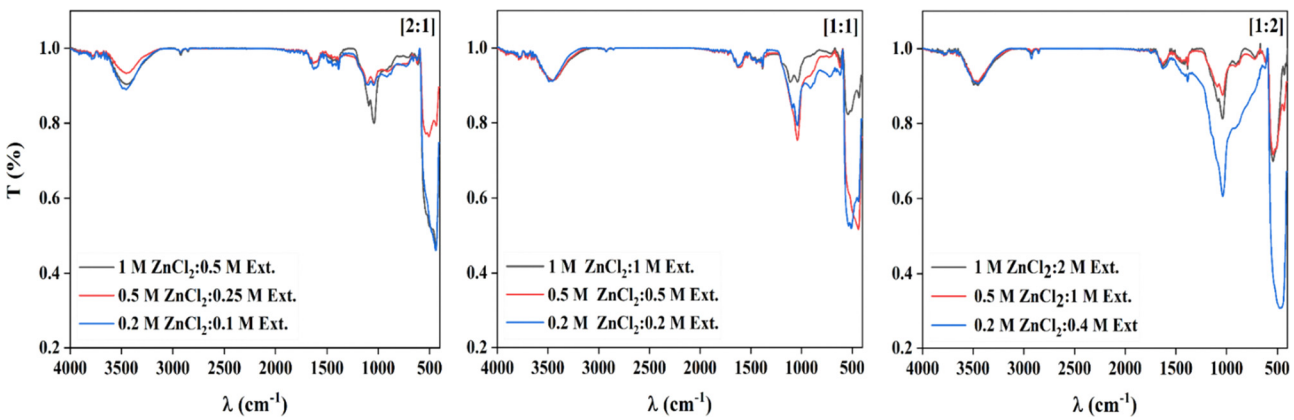

Fig. 5 FTIR spectrum of the ZnO-NPs synthesized using an eco-friendly *Phoenix dactylifera*. L., extract at different ratios ([2 : 1], [1 : 1] and [1 : 2]) and concentrations (0.1, 0.2, 0.4, 0.5, 1 and 2 M).

from the simultaneous activity of phenolic compounds (phytochemicals) remaining as antioxidant agents and zinc ions in ZnO-NPs as catalysts by transferring a single electron and a hydrogen atom or by releasing an oxygen atom.[53,62,63] Further studies indicated that bioactive compounds of the extracts were adsorbed onto nanoparticles.[64] Furthermore, research has demonstrated that nanoparticles have a higher total antioxidant activity than the standard (gallic acid).[65] For the anti-free radical DPPH activity, the optimum IC_{50} was attributed to the ZnO-NPs prepared at lower concentrations at each ratio (Table 1), which may be due to the lower-size nanoparticles.[66] Nevertheless, larger ZnO-NPs had polygonal or anisotropic structures and, as a result, exhibited a lower specific surface area, which reduced their reactivity with DPPH radicals; similar trends have been reported by K. Zar Myint *et al.*, 2021 and S. Pu *et al.*, 2019.[66,67] The ZnO-NPs synthesized using an eco-friendly *Phoenix dactylifera* L. extract exhibited strong antioxidant activity. As a standard, the IC_{50} value for gallic acid was determined to be 0.4 ± 0.2 mg mL^{-1}.

Antibacterial activity

Table 2 shows the inhibition areas of ZnO-NPs through their significant parameter (diameter).

The results were comparable to those of gentamicin (50 μg mL^{-1}). It was found that ZnO-NPs exhibited moderate antibacterial activity against pathogenic Gram-positive (*S. aureus*) and Gram-negative (*E. coli*) bacteria, with inhibition areas of up to 19 mm, as shown in Fig. 6.

The green synthesized ZnO-NPs with higher TAC presented a higher antibacterial activity than those with higher DPPH antiradical activity against both pathogenic strains. This could be due to the smaller size of the ZnO-NPs, which confers NPs with an excellent ability to inhibit the replication of bacterial DNA.[68,69] Small size of nano-scale particles allows them to penetrate the bacterial membranes and inactivate them by zero-valent metal oxide nanoparticles (ZVMONs), which then could oxidize intercellular oxygen, causing oxidative stress and cell membrane damage. The oxidative stress might be produced by reactive oxygen species (ROS), such as hydroxyl radicals (–OH), hydrogen peroxide (H_2O_2), singlet oxygen ($^1O_2$) and superoxide radicals (O^{2-}).[22,70] Bacteria are especially susceptible to ROS, which can damage their proteins and DNA. Both pathogenic bacteria (*S. aureus* and *E. coli*) were inhibited by ZnO-NPs investigated here, which could be a rich source of ROS. Similar reactions have been reported in the literature.[71–73] Nevertheless, the high antibacterial activity of ZnO-NPs could also be associated with their high crystallinity, which allows the released Zn^{+2} to collide with the negatively charged membranes of bacteria, thereby destroying their protein structure.[74,75]

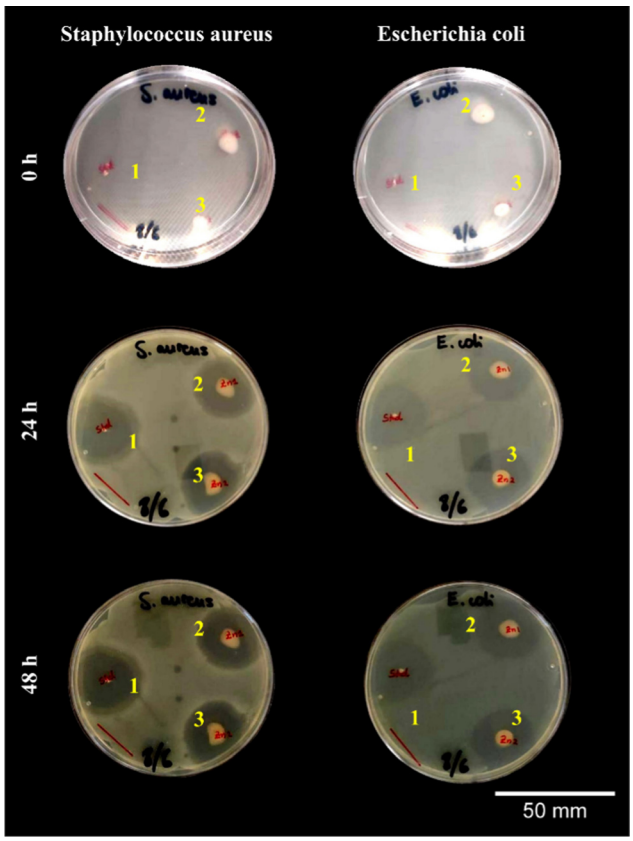

Fig. 6 Inhibition zones produced by 1. antibiotic gentamicin as a standard, 2. eco-synthesized ZnO-NPs [0.2 : 0.1] and 3. ZnO-NPs [0.2 : 04] against Staphylococcus aureus (*S. au*) and Escherichia coli (*E. coli*) over the time.

Table 2 Inhibition zones (represented by their diameter in mm) produced from eco-friendly synthesized ZnO-NPs against *Staphylococcus aureus* (*S. au*) and *Escherichia coli* (*E. col*). Gentamicin was used as a standard

Test time (h)	Samples	Inhibition diameter (mm)	
		Staphylococcus aureus	*Escherichia coli*
24	1 Gentamicin	28.3 ± 0.3^{a}	30.4 ± 0.7^{A}
	2 ZnO-NPs [0.2 : 0.1]	19.4 ± 0.2^{b}	21 ± 0.4^{B}
	3 ZnO-NPs [0.2 : 04]	18.2 ± 0.2^{c}	19.2 ± 0.6^{C}
48	1 Gentamicin	26.6 ± 0.1^{a}	28.1 ± 0.4^{A}
	2 ZnO-NPs [0.2 : 0.1]	17.7 ± 0.2^{b}	17.4 ± 0.7^{B}
	3 ZnO-NPs [0.2 : 04]	17.0 ± 0.1^{c}	16.4 ± 0.5^{B}

Note: Different superscript letters (a–c and A–B) within a column in a time row indicate significant differences among mean observations ($p < 0.05$).

Concluding remarks

The use of the *Phoenix dactylifera* L. extract in the synthesis of ZnO-NPs provides an excellent route for an eco-friendly method of manufacturing nanoparticles.

These nanoparticles appear to have a variety of shapes and structural features, and SEM examination revealed that nanoparticles aggregate and form networks depending on the concentration of both the precursor and the reducing agent used. ZnO-NPs synthesized from the *Phoenix dactylifera* L. extract have been shown to have high antioxidant activity caused by trapping of free radicals. Consequently,

nanotechnology-based antioxidants are difficult to compare across different cases, and the antioxidant capacity of NPs varies according to their size, crystallinity degree, shape, and concentration. In the presence of spherical NPs, the antioxidant activity may be higher than in those systems with irregular or polygonal NPs. Therefore, ZnO-NPs synthesized from the *Phoenix dactylifera* L. extract may be regarded as promising antibacterial drugs with great potential for the replacement of today's antibiotics.

The green synthesized ZnO-NPs through the use of eco-friendly *Phoenix dactylifera* L. extracts could be a potential substitute for NPs obtained using chemical methods not only due to a variety of benefits, related to process efficiency, cost-effectiveness and eco-friendliness, but also due to their reactivity and functionality (antioxidant capacity and antibacterial activity).

Author contributions

Conceptualization, J. A. A. A., A. R. and A. G.; methodology, J. A. A. A. and M. J. R.; software, J. A. A. A.; validation, J. A. A. A. and A. R.; formal analysis, M. J. R.; investigation, J. A. A. A. and M. J. R.; resources, A. G.; data curation, J. A. A. A; writing—original draft preparation, J. A. A. A. and M. J. R.; writing---review and editing, A. R. and A. G.; visualization, A. R. and A. G.; supervision, A. R. and A. G.; project administration, A. G.; and funding acquisition, A. G.

Conflicts of interest

The authors declare no conflict of interest.

Acknowledgements

The authors would like to acknowledge the MCI/AEI/FEDER, EU project (ref. RTI2018-097100-*B*-C21) that supported this work. In addition, the authors would also thank the predoctoral grant from J. A. A. A (Universidad de Sevilla, CODE 810) and M. J. R (Ministerio de Educación y Formación Profesional, FPU17/01718). J. A. A. A. would like to thank the support from the Hayel Saeed Anam group, represented by Abdul Jabbar Hayel Saeed Anam. The authors also thank CITIUS for granting access to and their assistance with the XRD area characterization and microscopy services.

References

1 M. Umadevi, M. R. Bindhu and V. Sathe, *J. Mater. Sci. Technol.*, 2013, **29**, 317–322.
2 D. R. Paul and L. M. Robeson, *Polymer*, 2008, **49**, 3187–3204.
3 M. H. Al-maamori, *J. Pure Appl. Sci.*, 2017, **25**, 497–503.
4 A. Kolodziejczak-Radzimska and T. Jesionowski, *Materials*, 2014, **7**, 2833–2881.
5 R. Wahab, I. H. Hwang, H.-S. Shin, Y.-S. Kim, J. Musarrat, A. A. Al-Khedhairy and M. A. Siddiqui, *Intelligent Nanomaterials*, John Wiley & Sons, Inc., Hoboken, NJ, USA, 2012, pp. 183–212.
6 H. Mirzaei and M. Darroudi, *Ceram. Int.*, 2017, **43**, 907–914.
7 A. Moezzi, A. M. McDonagh and M. B. Cortie, *Chem. Eng. J.*, 2012, **185–186**, 1–22.
8 A. M. Al-Mohaimeed, W. A. Al-Onazi and M. F. El-Tohamy, *Molecules*, 2022, **27**, 579.
9 C. Ashajyothi, K. H. Harish, N. Dubey and R. K. Chandrakanth, *J. Nanostruct. Chem.*, 2016, **6**, 329–341.
10 M. D. Fahmy, H. E. Jazayeri, M. Razavi, M. Hashemi, M. Omidi, M. Farahani, E. Salahinejad, A. Yadegari, S. Pitcher and L. Tayebi, *Intell. Nanomater.*, 2016, **13**, 199–245.
11 A. Singh, N. B. Singh, I. Hussain, H. Singh, V. Yadav and S. C. Singh, *J. Biotechnol.*, 2016, **233**, 84–94.
12 J. Wu, S. Chen, S. Ge, J. Miao, J. Li and Q. Zhang, *Food Hydrocolloids*, 2013, **32**, 42–51.
13 Z. Markova, P. Novak, J. Kaslik, P. Plachtova, M. Brazdova, D. Jancula, K. M. Siskova, L. Machala, B. Marsalek, R. Zboril and R. Varma, *ACS Sustainable Chem. Eng.*, 2014, **2**, 1674–1680.
14 W. Nakbanpote, M. Ruttanakorn, K. Sukadeetad, N. Sakkayawong and S. Damrianant, *ScienceAsia*, 2019, **45**, 127–137.
15 M. C. Karam, J. Petit, D. Zimmer, E. Baudelaire Djantou and J. Scher, *J. Food Eng.*, 2016, **188**, 32–49.
16 N. Toropov and T. Vartanyan, *Compr. Nanosci. Nanotechnol.*, 2019, 61–88.
17 F. M. Mohammadi and N. Ghasemi, *J. Nanostruct. Chem.*, 2018, **8**, 93–102.
18 G. S. Ghodake, N. G. Deshpande, Y. P. Lee and E. S. Jin, *Colloids Surf., B*, 2010, **75**, 584–589.
19 M. F. Zayed and W. H. Eisa, *Spectrochim. Acta, Part A*, 2014, **121**, 238–244.
20 G. Gajanan, M. Chang, J. Kim and E. Jin, *J. Mater. Sci.*, 2011, **46**, 4741–4747.
21 J. Rodríguez-Carvajal, *Phys. B*, 1993, **192**, 55–69.
22 N. Tran, A. Mir, D. Mallik, A. Sinha, S. Nayar and T. J. Webster, *Int. J. Nanomed.*, 2010, **5**, 277–283.
23 R. R. Krueger, *Date Palm Genetic Resources and Utilization*, Springer, Netherlands, Dordrecht, 2015, vol. 2, pp. 447–485.
24 N. Baazaoui and B. Sghaier-Hammami, in Green Synthesis of Nanoparticles from Date Palm (*Phoenix dactylifera*L.), ed. J. M. Al-Khayri, S.M. Jain and D.V. Johnson, *The Date Palm Genome, Compendium of Plant Genomes*, Springer, Cham, 2021, vol. 2, DOI: 10.1007/978-3-030-73750-4_3.
25 C. C. T. Chao and R. R. Krueger, *HortScience*, 2007, **42**, 1077–1082.
26 L. S. Eddine, L. Segni, G. Noureddine, O. M. Redha and M. Sonia, *Int. Lett. Chem., Phys. Astron.*, 2013, **14**, 125–135.
27 A. Mohamed and E. Shafey, *Green Process. Synth.*, 2020, **9**, 304–339.
28 A. Jayachandran, T. R. Aswathy and A. S. Nair, *Biochem. Biophys. Rep.*, 2021, **26**, 100995.

29 J. A. A. Abdullah, L. Salah Eddine, B. Abderrhmane, M. Alonso-González, A. Guerrero, A. Romero, J. A. Ahmed, L. Salah and B. Abderrhmane, *Sustainable Chem. Pharm.*, 2020, **17**, 100280.
30 J. A. A. Abdullah, M. Jiménez-Rosado, V. Perez-Puyana, A. Guerrero and A. Romero, *Nanomaterials*, 2022, **12**, 2449.
31 A. A. Barzinjy and H. H. Azeez, *SN Appl. Sci.*, 2020, **2**, 1–14.
32 I. Bibi, S. Kamal, A. Ahmed, M. Iqbal, S. Nouren, K. Jilani, N. Nazar, M. Amir, A. Abbas, S. Ata and F. Majid, *Int. J. Biol. Macromol.*, 2017, **103**, 783–790.
33 A. A. Ayachi, H. Mechakra, M. M. Silvan, S. Boudjaadar and S. Achour, *Ceram. Int.*, 2015, **41**, 2228–2233.
34 S. S. Behera, J. K. Patra, K. Pramanik, N. Panda and H. Thatoi, *World J. Nano Sci. Eng.*, 2012, **02**, 196–200.
35 J. A. A. Abdullah, M. Jiménez-Rosado, A. Guerrero and A. Romero, *Materials*, 2022, **15**, 1966.
36 J. Albertsson, S. C. Abrahams and Å. Kvick, *Acta Crystallogr., Sect. B: Struct. Sci.*, 1989, **45**, 34–40.
37 J. H. Park, C. Park, K. S. Lee and S. J. Suh, *AIP Adv.*, 2020, **10**(11), 115220.
38 H. Seok Kim, Y. S. Seo, K. Kim, J. W. Han, Y. Park and S. Cho, *Nanoscale Res. Lett.*, 2016, **11**(1), DOI: **10.1186/s11671-016-1393-x**.
39 D. Suresh, P. C. Nethravathi, C. Udayabhanu, M. A. Pavan Kumar, H. Raja Naika, H. Nagabhushana and S. C. Sharma, *Mater. Sci. Semicond. Process.*, 2015, **40**, 759–765.
40 X. Wang, D. P. Yang, P. Huang, M. Li, C. Li, D. Chen and D. Cui, *Nanoscale*, 2012, **4**, 7766–7772.
41 A. Fuad, A. A. Fibriyanti, Subakti, N. Mufti and A. Taufiq, *IOP Conf. Ser.: Mater. Sci. Eng.*, 2017, **202**(1), DOI: **10.1088/1757-899X/202/1/012074**.
42 R. Jon, N. Martin, P. R. Dasari, A. Paul and V. Singh, *Int. J. Eng. Adv. Technol.*, 2019, **9**, 870–873.
43 S. Hosseini Largani and M. Akbarzadeh Pasha, *Int. Nano Lett.*, 2017, **7**, 25–33.
44 J. Singh, T. Dutta, K.-H. Kim, M. Rawat, P. Samddar and P. Kumar, *J. Nanobiotechnol.*, 2018, **16**, 84.
45 K. S. Mukunthan and S. Balaji, *Int. J. Green Nanotechnol.*, 2012, **4**, 71–79.
46 A. J. Love, V. V. Makarov, O. V. Sinitsyna, J. Shaw, I. V. Yaminsky, N. O. Kalinina and M. E. Taliansky, *Front. Plant Sci.*, 2015, **6**, DOI: **10.3389/fpls.2015.00984**.
47 A. G. Vega-Poot, G. Rodríguez-Gattorno, O. E. Soberanis-Domínguez, R. T. Patiño-Díaz, M. Espinosa-Pesqueira and G. Oskam, *Nanoscale*, 2010, **2**, 2710–2717.
48 N. Andarini, R. S. Farida and T. Haryati, *Reaktor*, 2021, **21**, 45–51.
49 H. Shokry Hassan, A. B. Kashyout, H. M. A. Soliman, M. A. Uosif and N. Afify, *Angl. J.*, 2013, **3**, DOI: **10.0001/(AJ).V3I0.707.G857**.
50 M. Pudukudy and Z. Yaakob, *J. Cluster Sci.*, 2015, **26**, 1187–1201.
51 C. A. Soto-Robles, P. A. Luque, C. M. Gómez-Gutiérrez, O. Nava, A. R. Vilchis-Nestor, E. Lugo-Medina, R. Ranjithkumar and A. Castro-Beltrán, *Results Phys.*, 2019, **15**(9), DOI: **10.1016/j.rinp.2019.102807**.
52 P. N. Sibiya and M. J. Moloto, *Chalcogenide Lett.*, 2014, **11**, 577–588.
53 M. Junaid, H. Dowlath, S. Anjum, S. B. M. Khalith, S. Varjani, S. Kumar, G. Munuswamy, S. Woong, W. Jin and B. Ravindran, *Environ. Res.*, 2021, **201**, 111585.
54 C.-M. Hsu, Y.-H. Huang, H.-J. Chen, W.-C. Lee, H.-W. Chiu, J. P. Maity, C.-C. Chen, Y.-H. Kuo and C.-Y. Chen, *Mater. Today Commun.*, 2018, **14**, 302–311.
55 T. Wang, X. Jin, Z. Chen, M. Megharaj and R. Naidu, *Sci. Total Environ.*, 2014, **466–467**, 210–213.
56 B. Udvardi, I. J. Kovács, T. Fancsik, P. Kónya, M. Bátori, F. Stercel, G. Falus and Z. Szalai, *Appl. Spectrosc.*, 2017, **71**, 1157–1168.
57 K. Mohan Kumar, B. K. Mandal, K. Siva Kumar, P. Sreedhara Reddy and B. Sreedhar, *Spectrochim. Acta, Part A*, 2013, **102**, 128–133.
58 P. Salgado, K. Márquez, O. Rubilar, D. Contreras and G. Vidal, *Appl. Nanosci.*, 2019, **9**, 371–385.
59 Y. Khane, K. Benouis, S. Albukhaty, G. M. Sulaiman, M. M. Abomughaid, A. Al Ali, D. Aouf, F. Fenniche, S. Khane, W. Chaibi, A. Henni, H. D. Bouras and N. Dizge, *Nanomaterials*, 2022, **12**, 2013.
60 N. Z. Srećković, Z. P. Nedić, D. Liberti, D. M. Monti, N. R. Mihailović, J. S. Katanić Stanković, S. Dimitrijević and V. B. Mihailović, *RSC Adv.*, 2021, **11**, 35585–35599.
61 A. K. Keshari, R. Srivastava, P. Singh, V. B. Yadav and G. Nath, *J. Ayurveda Integr. Med.*, 2020, **11**, 37–44.
62 A. Demirbas, B. A. Welt and I. Ocsoy, *Mater. Lett.*, 2016, **179**, 20–23.
63 X. Zhao, L. Zhou, M. Shahid, R. Rajoka, L. Yan, D. Shao, J. Zhu, J. Shi, Q. Huang and H. Yang, *Crit. Rev. Biotechnol.*, 2018, **38**, 817–835.
64 F. Öztürk, S. Ço and F. Duman, *Mater. Sci. Eng. C Mater. Biol. Appl.*, 2020, **107**, 110207.
65 Z. Bedlovičová, I. Strapáč, M. Baláž and A. Salayová, *Molecules*, 2020, **25**, 1–24.
66 K. Zar Myint, Q. Yu, Y. Xia, J. Qing, S. Zhu, Y. Fang and J. Shen, *J. Food Sci.*, 2021, **86**, 284–292.
67 S. Pu, J. Li, L. Sun, L. Zhong and Q. Ma, *Carbohydr. Polym.*, 2019, **211**, 161–172.
68 L. M. Armijo, S. J. Wawrzyniec, M. Kopciuch, Y. I. Brandt, A. C. Rivera, N. J. Withers, N. C. Cook, D. L. Huber, T. C. Monson, H. D. C. Smyth and M. Osiński, *J. Nanobiotechnol.*, 2020, **18**, 1–27.
69 C. Lee, Y. K. Jee, I. L. Won, K. L. Nelson, J. Yoon and D. L. Sedlak, *Environ. Sci. Technol.*, 2008, **42**, 4927–4933.
70 S. A. Mahdy, Q. J. Raheed and P. T. Kalaichelvan, *Int. J. Mod. Eng. Res.*, 2012, **2**, 578–581.
71 D. Touati, *Arch. Biochem. Biophys.*, 2000, **373**, 1–6.
72 A. Datta, C. Patra, H. Bharadwaj, S. Kaur, N. Dimri and R. Khajuria, *J. Biotechnol. Biomater.*, 2017, **07**, 3–7.
73 A. M. Awwad and M. W. Amer, *Chem. Int.*, 2020, **6**, 210–2017.
74 P. Mohan and R. Mala, *Mater. Res. Express*, 2019, **6**(11), 115077.
75 C. Shuai, C. Wang, F. Qi, S. Peng, W. Yang, C. He, G. Wang and G. Qian, *J. Nanomater.*, 2020, **2020**, 1–12.